

# Integrated optical pattern generation on thin-film lithium niobate with electro-optic modulators and phase-change material cells

IVONNE BENTE,<sup>1</sup> FRANK BRÜCKERHOFF-PLÜCKELMANN,<sup>1</sup> J. RASMUS BANKWITZ,<sup>2</sup> DANIEL WENDLAND,<sup>1</sup> EMMA LOMONTE,<sup>1</sup> FRANCESCO LENZINI,<sup>1</sup> C. DAVID WRIGHT,<sup>3</sup> HARISH BHASKARAN,<sup>4</sup> AND WOLFRAM PERNICE<sup>1,2,\*</sup>

<sup>1</sup>*Institute of Physics, University of Münster, Heisenbergstr. 11, 48149 Münster, Germany*

<sup>2</sup>*Kirchhoff-Institute for Physics, Heidelberg University, Im Neuenheimer Feld 227, 69120 Heidelberg, Germany*

<sup>3</sup>*Department of Engineering, University of Exeter, Exeter, EX4 4QF, UK*

<sup>4</sup>*Department of Materials, University of Oxford, Parks Road, Oxford OX1 3PH, UK*

\*[wolfram.pernice@kip.uni-heidelberg.de](mailto:wolfram.pernice@kip.uni-heidelberg.de)

**Abstract:** Reconfigurable photonic integrated circuits enable high-bandwidth signal shaping with the prospect for scalability and compact footprint. Co-integration of electro-optical tunability with non-volatile attenuation through functional materials allows for implementing photonic devices which operate both on phase and amplitude. Based on this approach, we propose an integrated photonic design for optical pattern generation deploying a continuous-wave laser and a single electrical function generator. We employ the non-volatile and reconfigurable phase-change material Ge<sub>2</sub>Sb<sub>2</sub>Te<sub>5</sub> (GST) as a tunable attenuator for an integrated photonic circuit on the Lithium-Niobate-On-Insulator (LNOI) platform. The GST can be switched between its amorphous and crystalline phase, leading to an optical contrast of  $\cong 18$  dB. Combining this with integrated electro-optical modulators with a 4 GHz bandwidth in LNOI, enables the generation of short optical pulses, based on the principles of inverse discrete Fourier transform.

© 2022 Optica Publishing Group under the terms of the [Optica Publishing Group Open Access Publishing Agreement](#)

## 1. Introduction

Integrated optical pattern generation is a central task in several areas of photonic technologies, such as opto-microfluidic sensing [1], THz waveform synthesis [2], or radar applications [3]. Most approaches demonstrated so far for optical arbitrary waveform generation make use of frequency combs [4-6]. In a comb-based approach, each line must be wavelength-filtered and modulated coherently which requires precise fabrication for integrated wavelength multiplexing approaches, or even co-integration of photonic platforms is necessary [6]. Direct modulation is often challenging when the non-linear materials used for comb generation such as silicon nitride do not provide convenient physical mechanisms from high-frequency modulation. Therefore, alternative material platforms which enable signal shaping through the electro-optical effect are highly attractive. Besides continuous modulation approaches for high-frequency signal shaping, additional degrees of freedom for long-term stable reconfiguration is necessary. In this regard, non-volatile approaches which enable state retention over extended periods of time is required. Functional materials, such as phase-change materials (PCMs), have been very successful in this respect and are compatible with integrated photonic platforms.

In this work, we present a novel strategy for on-chip signal shaping where optical light pattern generation is enabled by the co-integration of electro-optic modulators (EOMs) and PCMs on the newly developed Lithium-Niobate-On-Insulator (LNOI) platform [7, 8]. Both PCMs and EOMs are already well-established components in integrated photonics for a wide range of applications [7-11]. PCMs have been frequently used in recent years in several

integrated photonic platforms, such as Si<sub>3</sub>N<sub>4</sub> [10, 11], or silicon-on-insulator [12] for optical data storage as well as high-bandwidth photonic computing. In addition, the non-volatile, and reconfigurable properties of the PCMs make them ideal for the implementation of variable integrated optical attenuators featuring minimal power consumption during continuous operation [10,11], while input power is only required during switching. EOMs, on the other hand, are fundamental building blocks for reconfigurable photonic circuits as they allow to convert fast electrical signals into the optical domain in a low loss fashion. More specifically, by leveraging on the high confinement of optical waveguides fabricated in the thin film lithium niobate (TFLN) material platform, LNOI-based electro-optic phase shifters have recently shown unprecedented performance, including modulation bandwidths up to  $\approx 100$  GHz, half-wave voltages in the single digit range, high signal-to-noise ratio, and insertion loss smaller than 0.25 dB/cm [9].

Combining PCM cells with EOMs on Lithium-Niobate-On-Insulator (LNOI) opens to the possibility of modifying simultaneously the phase as well as the amplitude of the travelling light. This can be exploited for realizing an optical pattern generator device based on the inverse discrete Fourier transform, as we propose here. Importantly, optical frequency shifting – a key ingredient for our inverse discrete Fourier transform device - has been experimentally demonstrated on TFLN-phase shifters [13]. Our design only requires a continuous-wave (cw) laser light source for optical input and it reduces the electrical interface and packaging requirements down to a single electrical function generator for the modulation of the phase shifter.

## 2. Device design for optical pattern generation

Discrete Fourier transform is widely used for signal processing [14-16]. In our approach we make use of the discrete Fourier transform to create optical patterns by calculating the discrete Fourier coefficients  $\widehat{a}_k$  of equidistantly sampled values  $a_n$  of a desired waveform. The discrete Fourier transform is defined as

$$\widehat{a}_k = \sum_{n=-(N-1)/2}^{(N-1)/2} e^{i2\pi kn/N} a_n, \text{ for odd } N, \quad (1)$$

where  $N$  is the number of equidistant samples, and  $k$  integer index referencing the respective Fourier coefficient. The coefficients  $\widehat{a}_k$  are in general complex and can be used to reconstruct a continuous function in time  $p(t)$ , characterized by a period  $T$ , as:

$$p(t) = \frac{1}{N} \sum_{k=-\frac{N-1}{2}}^{\frac{N-1}{2}} e^{\frac{i2\pi kt}{T}} \widehat{a}_k. \quad (2)$$

We design an integrated photonic approach to perform on-chip inverse discrete Fourier transform optically based on the concept shown in Fig. 1a. CW laser light from an external source is coupled into the photonic integrated circuit, and is then divided equally by cascaded beam splitters into several arms of the device. With reference to Fig. 1b, each arm consists of an integrated phase shifter and a PCM-based variable photonic attenuator. While the modulator is modulated actively and electrically driven, the PCM cell remains passive and is only programmed once per waveform generation. Afterwards, the light is combined again in a single path with a second network of beam splitters. As a result, the intensity pattern of light at the circuit output matches the waveform that was programmed into the PCM attenuators and modulators as Fourier coefficients. More specifically, each Fourier summand in [Eq. (2)] is created in one individual arm of the device, as shown in Fig. 1b in detail. The phase of each Fourier summand is programmed with an electro-optic phase shifter, while the absolute value of the complex coefficients  $a_k$  is controlled via optical attenuation through appropriate absorption in the PCM cell. The lengths of the phase shifters are integer multiples of the shortest phase shifter such that the respective  $V_\pi$  are integer multiple of the smallest  $V_\pi$  as well.

Applying a same modulation voltage  $V(t) = V_0 f(t)$  to all the phase shifters simultaneously, with  $f(t)$  being a linear function of time, allows us to express the electric field amplitude of the light at the output of the circuit as:

$$p(t) = \sum_{k=-\frac{N-1}{2}}^{\frac{N-1}{2}} e^{i\pi \frac{V_0}{V_\pi k} f(t)} e^{i\phi_{\hat{a}_k} \frac{|\hat{a}_k|}{N}}. \quad (3)$$

We use  $|\hat{a}_k|/N$  for the amplitude attenuation with the PCM cell and the phase  $\phi_{\hat{a}_k} = \arg(\hat{a}_k)$  is programmed into the phase shifter by a DC bias.

Upon a proper choice of  $V_0$  and with the  $V_\pi$  of the respective arms being integer multiple of each other, [Eq. (3)] becomes formally equivalent to [Eq. (2)], with the fraction  $V_0/V_\pi$  being equal to the index  $2k$  of the inverse discrete Fourier transform. Under this condition the same RF modulation  $f(t)$  can be applied to all of the phase shifters. One arm of the device does not have an integrated phase shifter to represent the summand for  $k = 0$  in [Eq. (3)]. In our proposed design every phase shifter length is repeated twice (see Fig. 1a), with the positions of signal and ground electrodes being inverted in the two halves of the device in order to apply phase shifts with opposite signs. This allows us to implement the summand  $-k$  in the lower part of the device, and the summand  $k$  in the upper part.

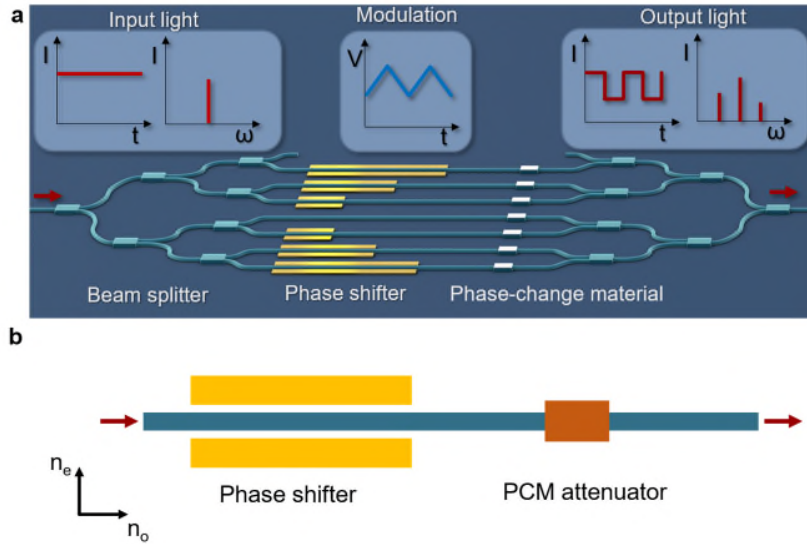


Fig. 1. Schematic illustration of the proposed device. a) The input light is a single-line laser with constant input. The light is guided through waveguides and split up in to several arms by beam splitters. In the respective arms the light passes a phase shifter and a phase-change material cell. At the end the light is combined by multi-mode interferometer and the generated pattern can be seen in the intensity, consisting of several frequencies. The phase shifter can be modulated by an RF voltage. b) The components of one device arm. The ordinary  $n_o$  and extraordinary  $n_e$  axis of the LNOI with respect to the orientation of the phase shifter is indicated by the arrows.

### 3. Integrated phase-change material and electro-optic modulators in LNOI

For the experimental realization of the proposed integrated optical pattern generator, LNOI is our material of choice because of its high modulation bandwidth - a key requirement for enabling the generation of ultra-short pulses. While the implementation of EOMs in LNOI is established and already achieved in several works [9,17], to demonstrate the possibility of

utilizing this platform for the proposed design, a key step is the integration of a PCM with LNOI waveguides, which so far has not been accomplished. We successfully fabricate a PCM cell in thin-film LN waveguides and co-integrate it with an electro-optic modulator.

The chalcogenide phase-change material chosen for our experiment is  $\text{Ge}_2\text{Sb}_2\text{Te}_5$  (GST). Optical circuits are implemented as ridge waveguides fabricated by electron-beam lithography and argon etching on a 300 nm thick X-cut LN film [17]. The top width of the waveguides is chosen equal to 1.1  $\mu\text{m}$  to ensure single-mode operation at telecom wavelength. The sidewall angle of the waveguides, resulting from our fabrication process, is approximately  $60^\circ$ . GST cells are deposited atop of the waveguides by DC-magnetron sputtering with a standard lift-off process. Fig. 2a shows, as an example, a false color SEM image of a 12 nm thick GST cell with a 1 nm adhesion and 5 nm capping layer of  $\text{Al}_2\text{O}_3$  (yellow) successfully deposited atop of a LNOI waveguide (blue). To achieve high absorption a GST cell of 4  $\mu\text{m}$  length along the propagation direction of the light is used. Fig. 2b shows the optical mode profiles of the beforementioned LNOI waveguide configuration with the GST on top. The different refractive index of the GST in the amorphous and crystalline phase leads to an absorption coefficient of  $\alpha_{\text{aGST}} = -0.07 \text{ dB}/\mu\text{m}$  in the amorphous phase and  $\alpha_{\text{cGST}} = -3.1 \text{ dB}/\mu\text{m}$  in the crystalline phase. The attenuation by the cell can be switched either optically in-plane through the waveguide [10], or out-of plane from the top using direct illumination with femtosecond laser pulses [18]. Changing the optical attenuation is done by modifying the phase state of the cell to suitable intermediate states between fully amorphous and fully crystalline. Switching the GST cell electrically by heaters has also been demonstrated [19]. By both approaches, the full device can be made reconfigurable.

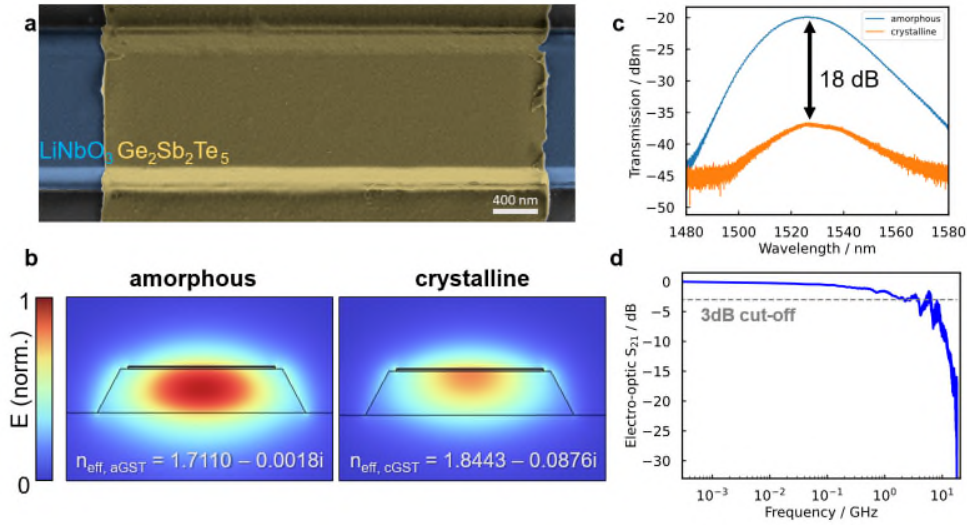


Fig. 2. a) False color SEM image of GST cell on top of a LNOI waveguide. b) Optical mode profiles with the effective refractive indices of amorphous and crystalline GST (12 nm) with a 1 nm adhesion and 5 nm capping layer of  $\text{Al}_2\text{O}_3$  on top of a LNOI waveguide with 300 nm height. c) Transmission measurement of a GST cell in the amorphous and crystalline phase. The optical contrast is  $\cong 18 \text{ dB}$ . d) Modulation bandwidth measurement of an integrated EOM on LNOI measured with a vector network analyzer at room temperature.

To evaluate the properties of the GST cells, light from a tunable CW laser is injected into a backloop with the integrated GST cell by employing surface grating couplers designed by following the approach of Ref. [20]. We found that in the as-deposited amorphous state the absorption of the GST is negligible, while in the crystalline state an optical contrast of 18 dB at 1530 nm is obtained as can be seen in Fig. 2c. Considering the measured optical contrast of

18 dB, we estimate that the normalized absolute value of the Fourier coefficients in [Eq. (1)] can be tuned in the range 0.016-1. On the same sample used for testing the properties of the GST cells, we realized a 1.7 mm long EOM in a push-pull configuration (see Ref. [17] for further details). The EOM displayed a half-wave voltage  $V_{\pi} \approx 15.5$  V and a 3 dB modulation bandwidth, measured with a vector network analyzer, equal to approximately 4 GHz (see Fig. 2d).

#### 4. Discussion

The previous analysis of the GST cell and EOM on LNOI for our proposed design provides the input parameters to estimate the optical pattern we expect to measure. Fig. 3 (i)-(iii) shows, as an example, the results for rectangular-, triangular-, and gaussian-shaped waveform. These pulses are sampled equidistantly with  $N = 7$ ,  $N = 15$ , and  $N = 31$  over the shown time range of 250 ps compliant with the bandwidth of the on-chip LNOI EOM. For the calculations the square root of the sampled values is determined before the discrete Fourier transform is performed.

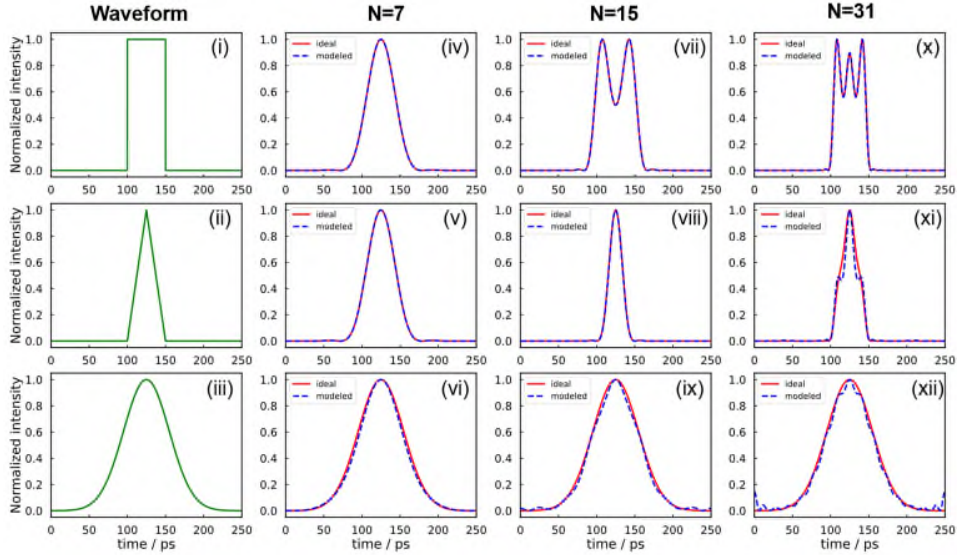


Fig. 3. Analytically calculated pulse shapes. In (i)-(iii) the ideal waveforms of a rectangular-, triangular-, and gaussian-shaped pulse are displayed. These waveforms are sampled with different  $N$  and Fourier transformed. For  $N = 7$  (iv)-(vi),  $N = 15$  (vii)-(ix), and  $N = 31$  (x)-(xii) the respective Fourier coefficients are used to calculate the resulting waveform of the proposed device (red curves). The blue curves show the pattern with Fourier coefficients corrected for the lower limit of the GST cell.

The images (iv)-(xii) in Fig. 3 show the resulting patterns plotted as a function of time for different sampling sizes, upon performing the inverse discrete Fourier transform via [Eq. (3)]. Here we use a triangular modulation function  $f(t)$  with a modulation frequency of 2 GHz for the phase shifters. The red curves in the figures represent the as-calculated function, in the ideal case in which the amplitudes  $|\hat{a}_k|/N$  can be tuned in the full range 0-1. The blue curve shows a more realistic expectation, as it accounts for  $|\hat{a}_k|/N$  limited to the range 0.016 – 1 as estimated from our measurements. For  $N = 7$  the pulse shape is similar for all three waveforms. Increasing the number of samples to  $N = 15$  improves the pulse shape especially for the triangular-shaped pulse as well as for the gaussian-shaped pulse. The rectangular-shaped pulse is better represented in its width, while there are still oscillations in the plateau. For  $N =$

31, the pulse shape for all three pulse shapes improves. With higher number of sampling points the influence of the lower boundary in transmission of the GST cell is more noticeable. At larger  $N$  a larger number of frequencies contribute to the final superposition but with a smaller Fourier coefficient. When using the GST cell as attenuator these coefficients are artificially enlarged, leading to a slight offset of the pattern from the desired outcome. Realizing the  $N = 31$  device would need 15 phase shifters with integer multiples of the smallest length. Assuming  $V_0 = 60$  V and a maximum  $V_\pi = 30$  V, the longest phase shifter would have a length of  $\cong 0.61$  cm, considering a  $V_\pi L \cong 2.6$  Vcm [17].

Our calculations and preliminary experimental measurements show that implementing discrete Fourier transformations by combining the electro-optic properties of LNOI and the non-volatile, reconfigurable nature of the PCMs, is a promising route for generating arbitrary optical patterns on-chip. We highlight that our strategy can greatly simplify current approaches to arbitrary optical waveform generation, reducing the required number of resources to a single CW laser and only one electrical waveform generator for modulation.

**Funding.** We acknowledge support by the Deutsche Forschungsgemeinschaft (DFG) through CRC 1459, the European Commission through grants CLUSTEC (101080173) and PINQS (724707) and the BMBF through grants PhoQuant, MUNIQ-Atoms and QSAMIS.

**Acknowledgments.** We thank Jochen Stuhmann from Illustrato for assistance with the graphical illustrations.

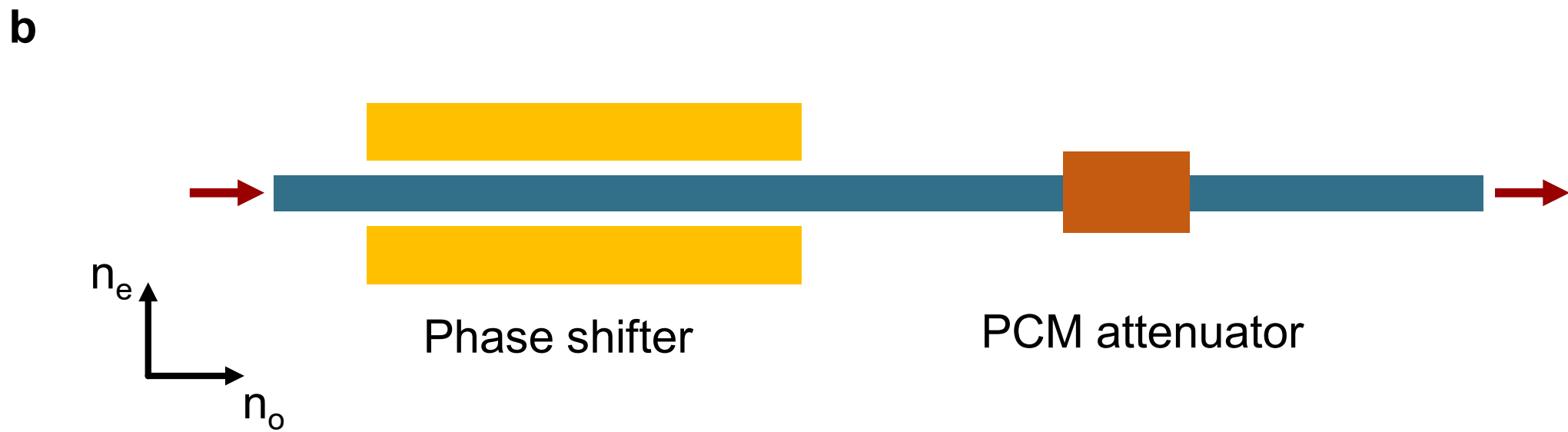
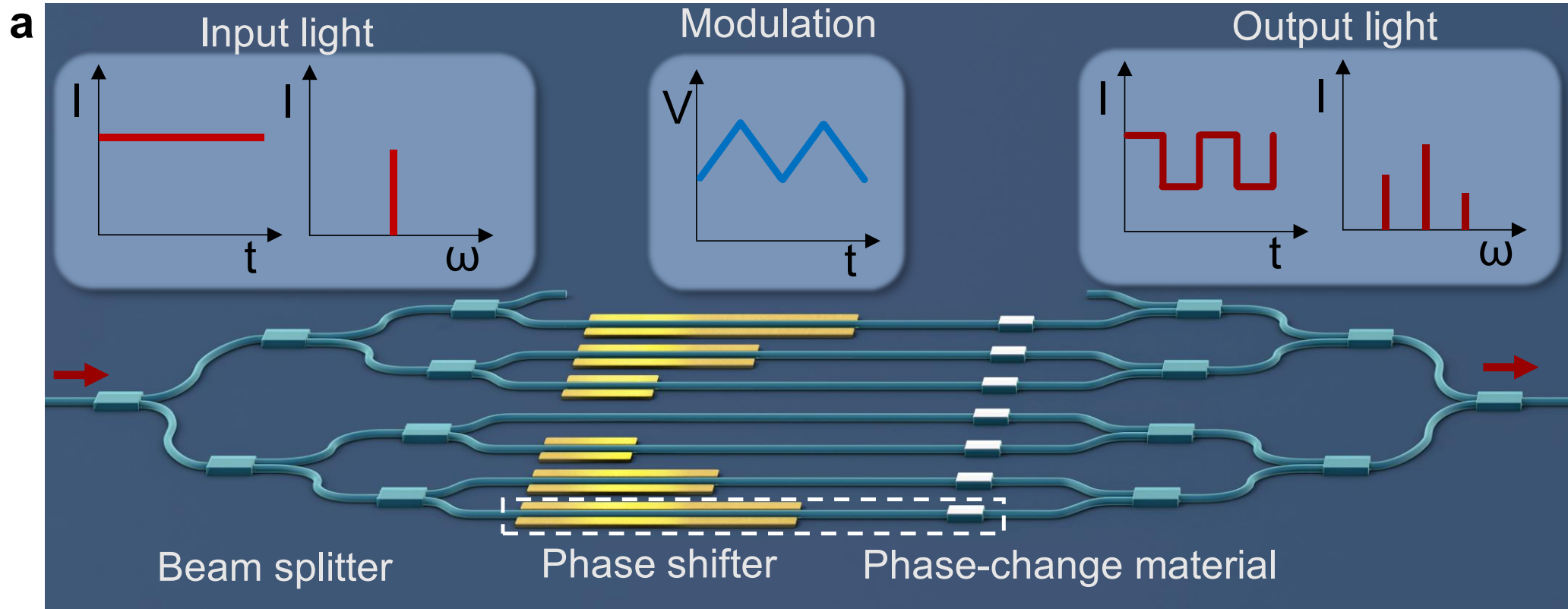
**Disclosures.** The authors declare no competing financial interests.

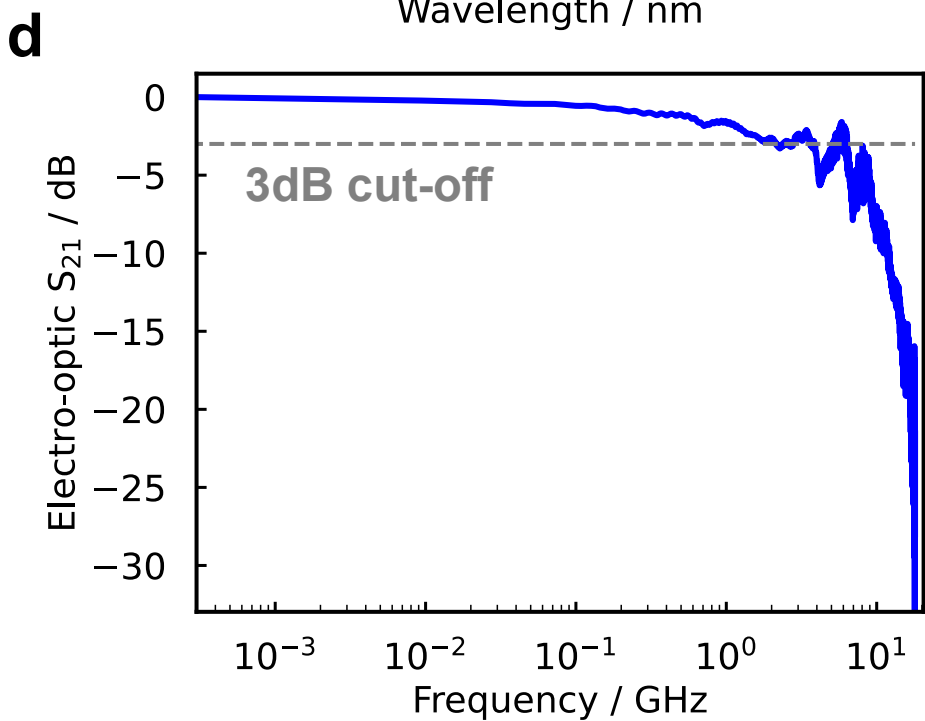
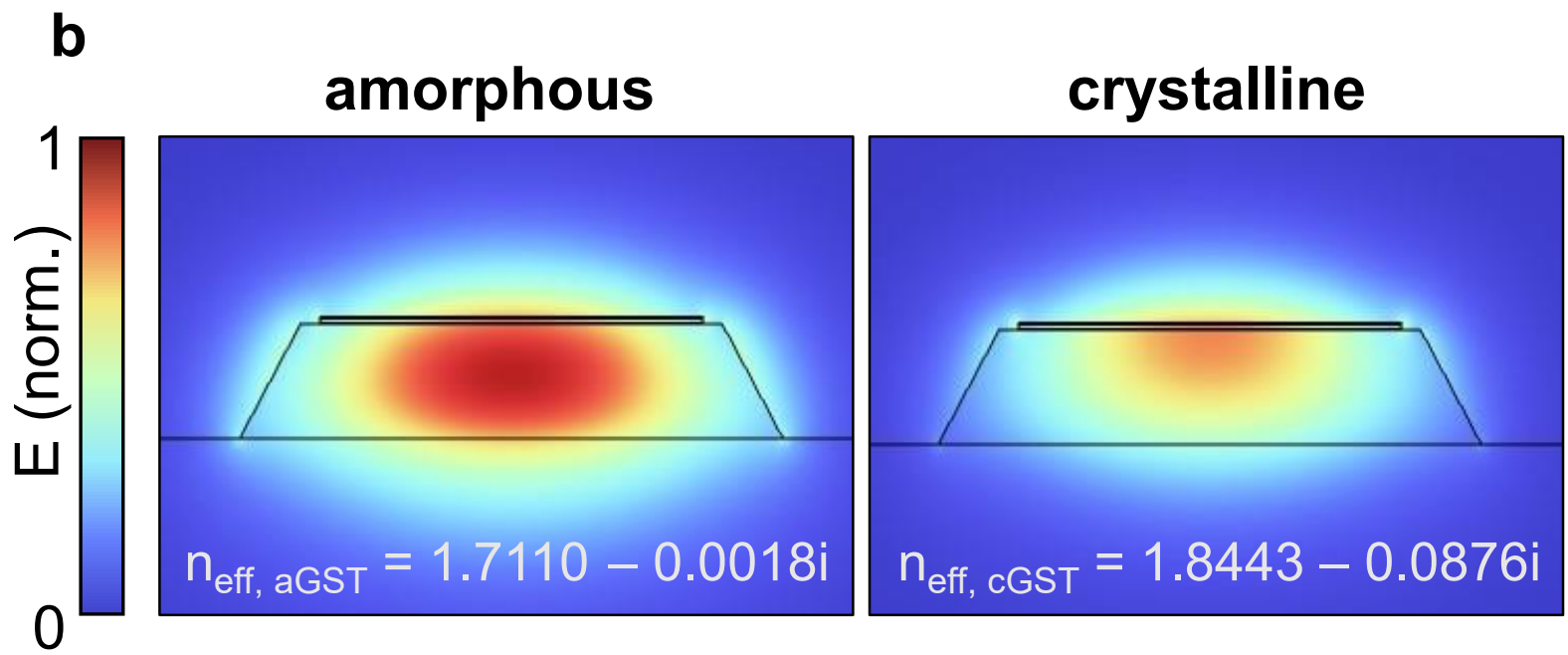
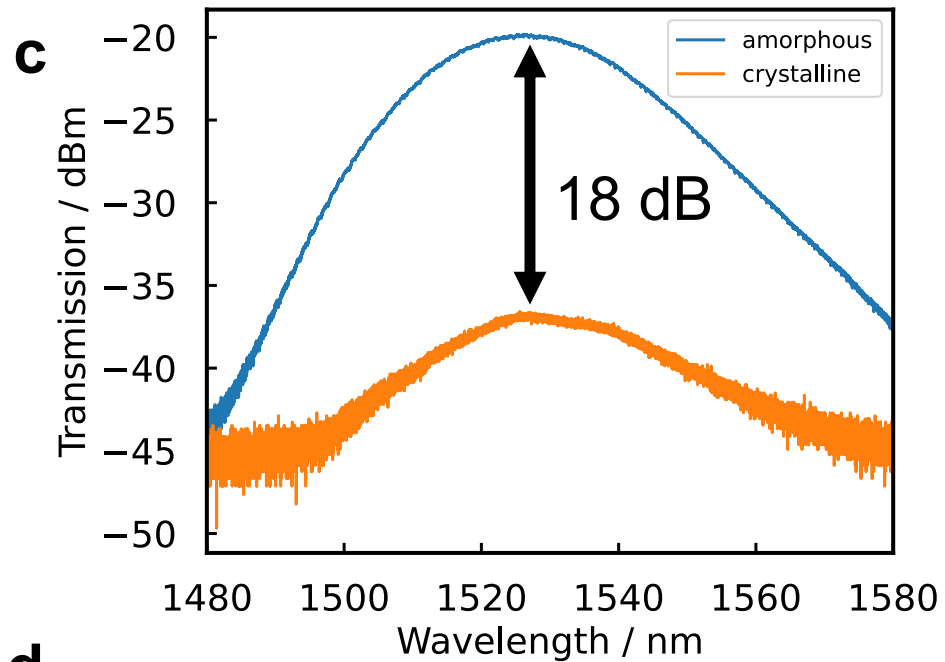
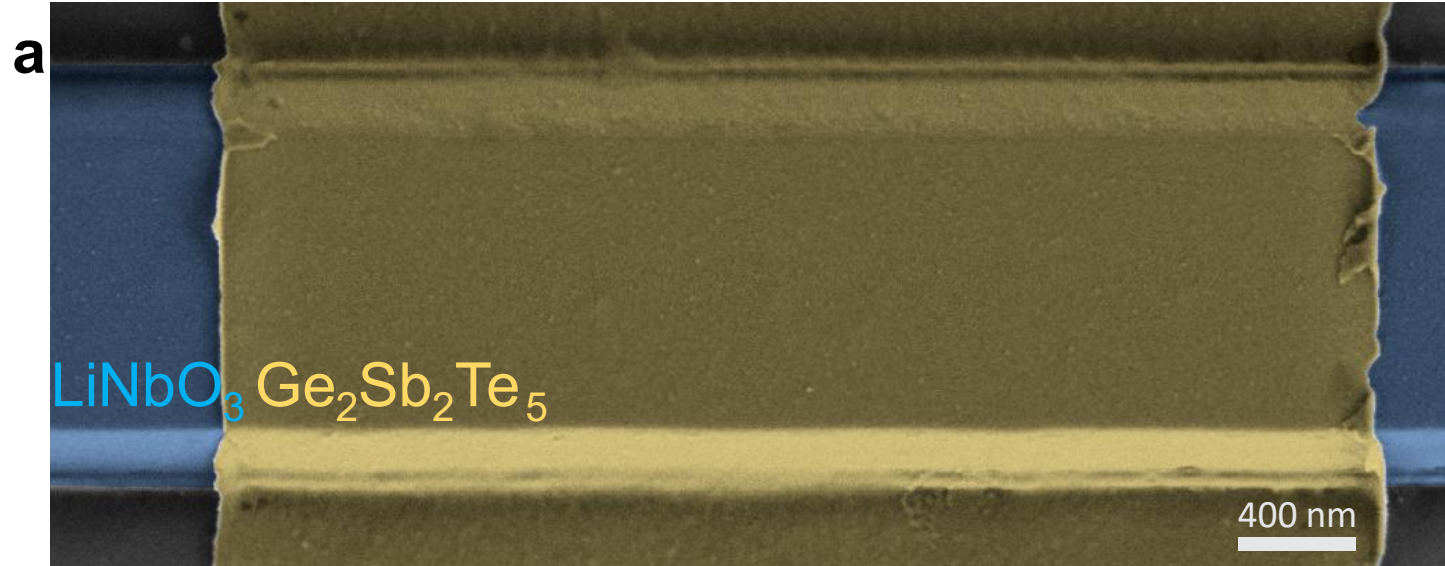
**Data availability.** Data is available from the authors upon reasonable request.

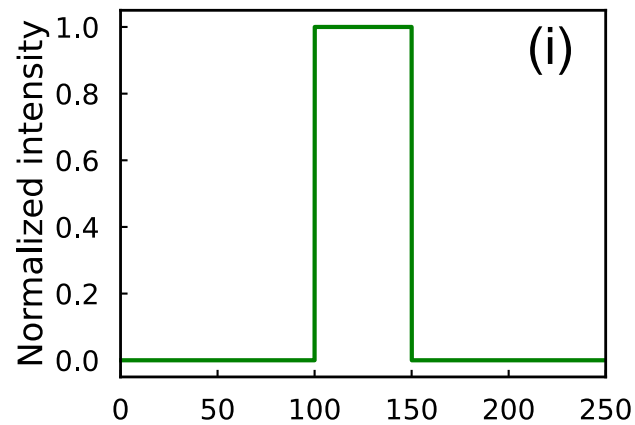
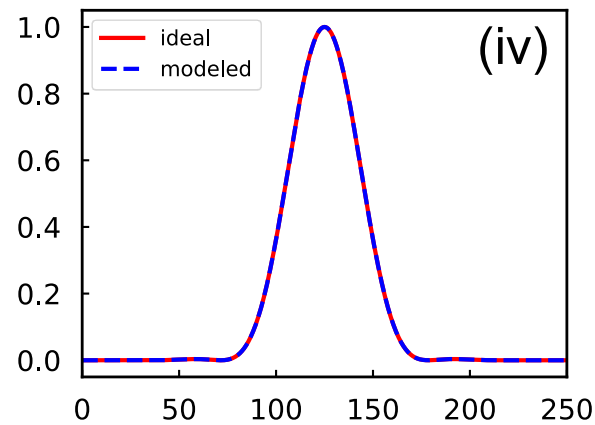
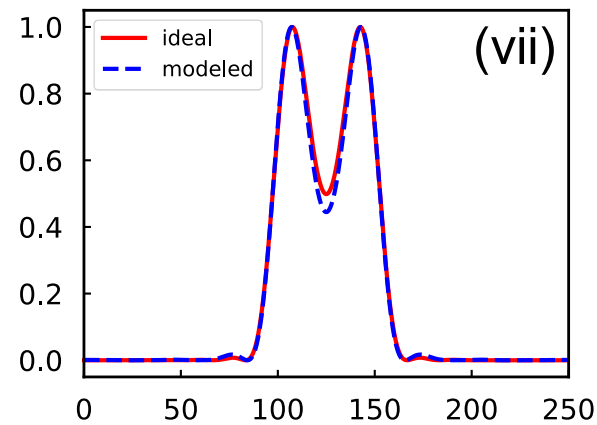
## References

- G. Bettella, R. Zamboni, G. Pozza, A. Zaltron, C. Montecchi, M. Pierno, G. Mistura, C. Sada, L. Gauthier-Manuel, and M. Chauvet, "LiNbO<sub>3</sub> integrated system for opto-microfluidic sensing," *Sensors and Actuators B: Chemical* **282**, 391-398 (2019).
- A. Herter, A. Shams-Ansari, F. F. Settembrini, H. K. Warner, J. Faist, M. Lončar, and I.-C. Benea-Chelmus, "Terahertz waveform synthesis in integrated thin-film lithium niobate platform," *Nat Commun* **14**, 11 (2023).
- M. H. Khan, H. Shen, Y. Xuan, L. Zhao, S. Xiao, D. E. Leaird, A. M. Weiner, and M. Qi, "Ultrabroad-bandwidth arbitrary radiofrequency waveform generation with a silicon photonic chip-based spectral shaper," *Nature Photon* **4**, 117-122 (2010).
- S. Liao, Y. Ding, J. Dong, T. Yang, X. Chen, D. Gao, and X. Zhang, "Arbitrary waveform generator and differentiator employing an integrated optical pulse shaper," *Opt. Express* **23**, 12161-12173 (2015).
- S. Cundiff, and A. Weiner, "Optical arbitrary waveform generation," *Nature Photon* **4**, 760-766 (2010).
- S. Feng, C. Qin, K. Shang, S. Pathak, W. Lai, B. Guan, M. Clements, T. Su, G. Liu, H. Lu, R. P. Scott, and S. J. B. Yoo, "Rapidly reconfigurable high-fidelity optical arbitrary waveform generation in heterogeneous photonic integrated circuits," *Opt. Express* **25**, 8872-8885 (2017).
- H. Hu, J. Yang, L. Gui, and W. Sohler, "Lithium niobate-on-insulator (LNOI): status and perspectives," *Proc. SPIE* **8431**, 84311D (2012).
- G. Poberaj, H. Hu, W. Sohler, and P. Günter, "Lithium niobate on insulator (LNOI) for micro-photonics devices," *Laser & photonics reviews* **6**(4), 488-503 (2012).
- C. Wang, M. Zhang, X. Chen, M. Bertrand, A. Shams-Ansari, S. Chandrasekhar, P. Winzer, and M. Lončar, "Integrated lithium niobate electro-optic modulators operating at CMOS-compatible voltages," *Nature* **562**, 101-104 (2018).
- C. Ríos, N. Youngblood, Z. Cheng, M. Le Gallo, W. H. P. Pernice, C. D. Wright, A. Sebastian, and H. Bhaskaran, "In-memory computing on a photonic platform," *Science Advances* **5**(2), eaau5759 (2019).
- J. Feldmann, N. Youngblood, M. Karpov, H. Gehring, X. Li, M. Stappers, M. Le Gallo, X. Fu, A. Lukashchuk, A. S. Raja, J. Liu, C. D. Wright, A. Sebastian, T. J. Kippenberg, W. H. P. Pernice, and H. Bhaskaran, "Parallel convolutional processing using an integrated photonic tensor core," *Nature* **589**, 52-58 (2021).
- S. Aggarwal, T. Milne, N. Farmakidis, J. Feldmann, X. Li, Y. Shu, Z. Cheng, M. Salinga, W. H. P. Pernice, and H. Bhaskaran, "Antimony as a Programmable Element in Integrated Nanophotonics," *Nano Lett.* **22** (9), 3532-3538 (2022).
- D. Zhu, C. Chen, M. Yu, L. Shao, Y. Hu, C. J. Xin, M. Yeh, S. Ghosh, L. He, C. Reimer, N. Sinclair, F. N. C. Wong, M. Zhang, and M. Lončar, "Spectral control of nonclassical light pulses using an integrated thin-film lithium niobate modulator," *Light Sci Appl* **11**, 327 (2022).
- M. J. Corinthis, "A Fast Fourier Transform for High-Speed Signal Processing," *IEEE Transactions on Computers*, C-20 (8), 843-846 (1971).

248 15. T. Ran, D. Bing, and W. Yue, "Research progress of the fractional Fourier transform in signal processing,"  
249 Science in China Series F 49, 1-25 (2006).  
250 16. L. R. Rabiner, and B. Gold, "Theory and application of digital signal processing", Englewood Cliffs: Prentice-  
251 Hall (1975).  
252 17. E. Lomonte, M. A. Wolff, F. Beutel, S. Ferrari, C. Schuck, Wolfram H. P. Pernice, and F. Lenzini, "Single-  
253 photon detection and cryogenic reconfigurability in lithium niobate nanophotonic circuits," Nat Commun **12**,  
254 6847 (2021).  
255 18. A. Ahmadiwand, B. Gerislioglu, R. Sinha, M. Karabiyik, and N. Pala, „Optical Switching Using Transition from  
256 Dipolar to Charge Transfer Plasmon Modes in Ge<sub>2</sub>Sb<sub>2</sub>Te<sub>3</sub> Bridged Metallodielectric Dimers," Sci Rep **7**, 42807  
257 (2017).  
258 19. Z. Fang, R. Chen, J. Zheng, A. I. Khan, K. M. Neilson, S. J. Geiger, D. M. Callahan, M. G. Moebius, A.  
259 Saxena, M. E. Chen, C. Rios, J. Hu, E. Pop, and A. Majumdar, "Ultra-low-energy programmable non-volatile  
260 silicon photonics based on phase-change materials with graphene heaters," Nat. Nanotechnol. **17**, 842-848  
261 (2022).  
262 20. E. Lomonte, F. Lenzini, and W. H. P. Pernice, "Efficient self-imaging grating couplers on a lithium-niobate-on-  
263 insulator platform at near-visible and telecom wavelengths," Opt. Express **29**, 20205-20216 (2021).





**Waveform****N=7****N=15****N=31**